

The Relationship Between Urban 2-D/3-D Landscape Pattern and Nighttime Light Intensity

Bin Wu , Chengshu Yang , Zuoqi Chen , *Member, IEEE*, Qiusheng Wu , Siyi Yu, Congxiao Wang, Qiaoxuan Li , Jianping Wu , and Bailang Yu , *Senior Member, IEEE*

Abstract—As spatial and socioeconomic processes are the two key aspects of urban development, revealing the relationship between these two key aspects is critical. Previous studies attempted to explain their correlation at the city or region level using built-up area metrics and nighttime light (NTL) data. However, more comprehensive studies on urban interior spatial characteristics and their relationship to NTL intensity are lacking in a three-dimension space. Using Luojia 1-01 nighttime light data, LiDAR digital surface model data, and other auxiliary data, this study applies an extreme gradient boosting regression model and Sharpley Additive exPlanations method to model and interpret the relationship between two-dimensional (2-D)/3-D landscape patterns and NTL intensity. Two study areas were selected to investigate the landscape–NTL relationship at the parcel and subdistrict levels. The major findings of this study include the following: 1) 2-D and 3-D urban landscape patterns have a close relationship with NTL intensity at the parcel and subdistrict scales; 2) the combinational metric of 2-D and 3-D landscape patterns has a stronger relationship with NTL intensity than either the 2-D or 3-D landscape metrics alone; 3) the correlations between most landscape metrics and NTL intensity are not simply positive or negative but change as metrics grow; and 4) the urban socioeconomic level is not only related to a single landscape metric sometimes but tends to the result of metrics interaction. These findings may help urban planners and government officials make more reasonable urban landscape planning policies under the goal of sustainable development.

Index Terms—Landscape metrics, nighttime light (NTL) data, three-dimensional (3-D) landscape pattern, urban development, extreme gradient boosting (XGBoost) regression.

Manuscript received October 31, 2021; revised December 10, 2021; accepted December 12, 2021. Date of publication December 15, 2021; date of current version January 3, 2022. This work was supported in part by the National Natural Science Foundation of China under Grant 41801343, Grant 42001357, and Grant 41871331, in part by the Shanghai Sailing Program under Grant 19YF1413800, in part by the China Postdoctoral Science Foundation under Grant 2020M671921 and Grant 2021T140207, and in part by the Fundamental Research Funds for the Central Universities of China. (*Corresponding author: Bailang Yu.*)

Bin Wu, Chengshu Yang, Congxiao Wang, Qiaoxuan Li, Jianping Wu, and Bailang Yu are with the Key Laboratory of Geographic Information Science (Ministry of Education) and the School of Geographic Sciences, East China Normal University, Shanghai 200241, China (e-mail: bwu@geo.ecnu.edu.cn; yjack90824@gmail.com; cxwang1992@126.com; leejoetion@gmail.com; jpwu@geo.ecnu.edu.cn; blyu@geo.ecnu.edu.cn).

Zuoqi Chen is with the Key Laboratory of Spatial Data Mining and Information Sharing of Ministry of Education, National & Local Joint Engineering Research Center of Satellite Geospatial Information Technology, and the Academy of Digital China, Fuzhou University, Fuzhou 35002, China (e-mail: zqchen@fzu.edu.cn).

Qiusheng Wu is with the Department of Geography, University of Tennessee, Knoxville, TN 37996 USA (e-mail: qwu18@utk.edu).

Siyi Yu is with the School of Economics and Management, Shanghai University of Sport, Shanghai 200438, China (e-mail: yusiyi@sus.edu.cn).

Digital Object Identifier 10.1109/JSTARS.2021.3135488

I. INTRODUCTION

THE world is becoming an urban planet. About 55% of the world's population has been living in urban areas since 2007, and that share is expected to increase to 68% by 2050 [1]. Rapid urbanization can result in various environmental consequences, such as excessive resource consumptions [2], worsening environmental pollution [3], inadequate urban services [4], and extreme urban heat conditions [5]–[8]. Understanding urban development and building sustainable cities have become an important part of the sustainable development goals of the United Nations, especially for developing countries where 95% of urban expansion are expected to take place in the next decades.

Although urbanization is usually defined as population increases in cities versus rural areas, urban development is a complex process and contains two key aspects: spatial and socioeconomic. Clarifying the relationship between these two aspects can contribute to sustainable urban development for policymakers and city planners. Previous studies revealed a strong correlation between urban spatial and socio-economic development, and it has been a long-standing notion that urban expansion and socioeconomic development can promote each other [9]–[12]. In the recent decade, furthermore, studies found that they have different causalities at different spatial and temporal scales. For example, Bai *et al.* [13] showed that there is a long-term bidirectional causality between GDP per capita and built-up areas in China at both provincial and city levels, and a short-term bidirectional causality that is stronger in larger and richer cities than smaller and poorer ones at the provincial level. At regional, urban agglomeration, and metropolitan scales, Shi *et al.* [14] argued a slightly different point that there are long-term bidirectional causality and short-term unidirectional causality from socioeconomic development to spatial expansion. These studies have revealed the causality between urban horizontal spatial development and socioeconomic level. Yet, urban spatial development is not only horizontal but vertical [15].

Global cities experienced varying degrees of vertical urban structure changes, especially in developing countries, such as China [16]. Remote sensing has been a powerful tool for extracting urban vertical information. Many remote sensing datasets, such as LiDAR data and high-resolution satellite images, have been used to extract urban three-dimensional (3-D) spatial characteristics [17]–[20]. Based on these 3-D details of urban vertical development, previous studies attempted to analyze the relationship between vertical urban development and socioeconomic factors. Zhang *et al.* [21] detected the horizontal

and vertical urban growth in Guangzhou and found they were strongly associated with the increases of three major socioeconomic indicators. Zambon *et al.* [22] proposed an index to derive the vertical to horizontal growth ratio and found it was associated with population density and increase in Greece. However, these studies largely focused on urban growth but not the urban spatial characteristics at the city level. The urban internal spatial structure has been proved significant in urban sustainable development [23]–[25]. Therefore, more comprehensive studies of urban interior spatial characteristics and their relationship to the socioeconomic level are required.

Landscape metrics have been widely used for characterizing urban landscape patterns. Quantifying the spatial characteristics for varied land covers at different scales, urban landscape metrics provide a better understanding of urban spatial development than urban growth rates [26], [27]. Moreover, besides the widely used 2-D landscape metrics, 3-D landscape metrics have been considered in a few urban analyses [28]–[30]. Therefore, urban landscape metrics are appropriate for quantifying 2-D and 3-D urban spatial patterns in this study. As for the finer resolution urban socioeconomic feature, nighttime light (NTL) remote sensing data that can reflect human socioeconomic activities is a good proxy data [31], [32]. NTL data have been widely used to estimate socioeconomic indices comprising population [33], [34], gross domestic product [35], [36], CO₂ emission [37], [38], electric power consumption [39], [40], total freight traffic [41], [42], urban structures [43], [44], and poverty [45]–[47]. Compared with the Defense Meteorological Satellite Program’s Operational Linescan System (DMSP-OLS) and the Suomi National Polar-orbiting Partnership’s Visible Infrared Imaging Radiometer Suite (NPP-VIIRS), the new generation of the nighttime light remote sensing satellite, Luojia 1-01, can provide higher quality NTL data, which attain more comprehensive information on human activities [48]–[50].

Landscape patterns are important for understanding the spatial structure and characteristics of urban environments. Previous studies [51], [52] reported that NTL intensity is sensitive to urban landscape patterns. In this context, considering the relationship between landscape pattern and NTL intensity is a key prerequisite for addressing linkages between urban growth and NTL-linked socioeconomic indicators. Therefore, it is necessary to explore the relationship between urban landscape patterns and NTL intensity. This article attempts to reveal the association between 2-D/3-D urban spatial patterns and NTL intensity at the parcel and subdistrict levels, and address two questions: 1) How are these 2-D and 3-D landscape metrics related to NTL intensity? 2) Do these landscape metrics interact with each other?

The rest of this article is organized as follows. Section II introduces the study area and datasets used in this study. In Section III, we subsequently explain a four-step framework to analyze the relationship between the 2-D/3-D urban spatial development and NTL intensity with an extreme gradient boosting (XGBoost) regression model and Sharpley Additive exPlanations (SHAP) method. The results of the model are presented in Section IV. Then, in Section V, we discuss and analyze the relationship between 2-D/3-D urban landscape patterns and the average NTL intensity at the parcel and subdistrict levels in two study areas

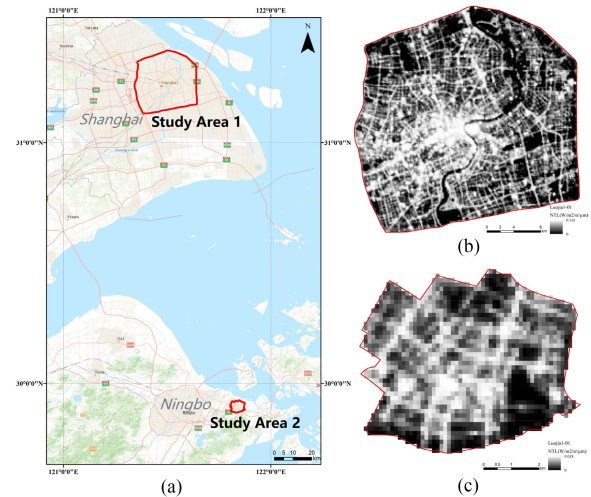


Fig. 1. Study areas. (a) Location of the two study areas. (b) NTL map of study area 1—Shanghai. (c) NTL map of study area 2—Ningbo, China.

and try to provide a scientific reference for government officials and urban planners. Finally, Section VI concludes the article.

II. STUDY AREA AND DATASETS

A. Study Area

Two study areas, Shanghai and Ningbo, China, were selected in this study. Shanghai is located in the Yangtze River Delta’s world-class urban agglomeration and has been the economic, trade, and technological innovation center of China. The fusion of booming development and multiculture provides Shanghai, especially the inner area of the main city (IMC), rich diversities of urban landscapes that few Chinese cities have. Therefore, we selected IMC as study area 1, which is surrounded by the outer ring road with an area of 664 km² [see Fig. 1(a)]. Ningbo is located in the southeastern part of East China’s Zhejiang province and the southern wing of the developed Yangtze River Delta region. Beilun district, the biggest district in Ningbo, is on the shore of the east side of Ningbo city. Beilun District is famous for its deep-water port, which is an important base for energy, raw material, and export-oriental processing. Compared with Shanghai IMC, the Beilun district is an underdeveloped area. In our study, the Beilun district was selected as study area 2. To avoid oversegmentation of the urban landscape, we chose parcels and subdistricts as the basic units of this study. Parcels are defined as polygons bounded by road networks and considered as the natural segmentation of urban areas [53], [54], while a subdistrict is an administrative division that is generally smaller than a district.

B. Datasets

Four datasets were used in this study, including Luojia 1-01 nighttime light data, digital surface model (DSM) of IMC, land cover map of Shanghai for landscape metrics calculation, and OpenStreetMap data for generating parcel polygons.

The Luojia 1-01 satellite was launched on June 2, 2018, which can acquire a global NTL image within 15 days. It has a finer

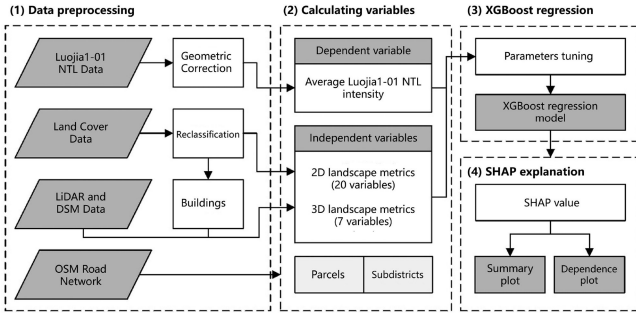


Fig. 2. Flowchart of analyzing the relationship between 2-D/3-D landscape patterns and NTL intensity.

spatial resolution (~ 130 m) than the two widely used nighttime light datasets, i.e., DMSF-OLS (~ 2.7 km) and NPP-VIIRS (~ 750 m). We downloaded the Luojia 1-01 nighttime light data of July 14, 2018, from the High-Resolution Earth Observation System of the Hubei Data and Application Center.¹

The DSM of Shanghai IMC was produced from high-resolution airborne image stereo pairs obtained in January 2016 with a spatial resolution of 0.5 m, provided by the Shanghai Surveying and Mapping Institute. The DSM of the Beilun district was generated using the method proposed by Wu *et al.* [55] from airborne LiDAR data, which was collected in December 2015 by the Ningbo Bureau of Natural Resources and Planning.

The land cover dataset was generated with the multiangle high-resolution satellite imagery acquired in September 2016 and other auxiliary data [56], [57]. It has a resolution of 2.5 m and seven land cover types, namely grass/shrubs, tree, bare soil, building, water, road, and other impervious surface areas (OISA), whose overall accuracy reached about 93% [58]. In this study, the land cover dataset was used to calculate 2-D landscape metrics and 3-D landscape metrics combined with the DSM.

OpenStreetMap (OSM,²) provides free road network data, including road shapefiles and corresponding road types, which were used to extract parcel polygons for Shanghai IMC and the Beilun district.

III. METHOD

In this study, we analyzed the relationship between 2-D/3-D landscape metrics and the average NTL intensity at the parcel and sub-district levels based on an XGBoost regression. As outlined in Fig. 2, our method consists of the following four steps.

- 1) Data preprocessing.
- 2) The parcel-level and subdistrict-level average NTL intensity from Luojia 1-01 were calculated as the dependent variable, and the 2-D/3-D landscape metrics were calculated as the independent variables.
- 3) An XGBoost regression was used to examine the relationship between the two levels of 2-D/3-D landscape metrics and the average NTL intensity.
- 4) The SHAP method was employed to study how the 2-D/3-D landscape metrics are correlated to NTL intensity.

A. Data Preprocessing

First, all data were projected into the WGS84 Web Mercator (Auxiliary Sphere) projection. To segment parcels, we selected motorways, trunk roads, primary, secondary, and tertiary roads from the OSM road network data, and set the road widths as 30, 30, 20, 17, and 10 m, respectively, following the study by Wang *et al.* [48]. Then parcels were obtained by removing road spaces from the study areas. We excluded parcels smaller than 0.02 km², which resulted in 1299 and 106 parcels in Shanghai IMC and the Beilun district, respectively.

Due to the slight geo-referencing error of Luojia1-01 NTL data, a geometric correction was carried out to reduce geometric errors based on the OSM road network data [48]. Besides, the original Luojia1-01 data were stored in INT32 format. Therefore, we converted the digital number (DN value) of original images to radiance via the following:

$$L = DN^{2/3} \cdot 10^{-10} \quad (1)$$

where L is the NTL radiance with the unit of $W/m^2/sr/\mu m$, and DN represents the pixel value.

For the land cover dataset, we combined “grass/shrubs” and “tree” as “vegetation.” Since roads were removed when we produced the parcels, the type “road” was also removed from the classification system. Then, we extracted building pixels from the land cover map for calculating 3-D landscape metrics.

B. Calculation of 2-D/3-D Landscape Metrics and NTL Intensity at the Two Levels

We calculated a group of 2-D/3-D landscape metrics to characterize urban landscape patterns (see Table I), taking the parcels and subdistricts as the basic units. Five widely used 2-D landscape metrics were applied to measure the spatial pattern of each land cover type: percentage of landscape (PLand), edge density (ED), largest patch index (LPI), patch density (PD), and percentage of like adjacency (PLADJ), which can describe the area proportion, the shape complexity, the spatial dominance of each class, the number of patches, and the degree of aggregation of the focal land cover type in each unit. We computed PLand, ED, LPI, PD, and PLADJ for four land cover types (building, OISA, bare soil, and vegetation) using FRAGSTATS 4.2 [59], and discarded the type “Water” with very few pixels. As a result, we obtained 20 2-D landscape metrics altogether in each parcel.

As we only focused on the 3-D landscape metrics of buildings, seven 3-D landscape metrics were calculated in ArcGIS 10.4 to measure the 3-D properties of buildings: total volume (TV), mean height (MH), height variance (HV), normalized height variance (NHV), 3-D percentage of landscape (3DPLand), 3-D largest patch index (3DLPI), and cubic index (CI). TV and MH indicate the space and height status of buildings in a unit, respectively. HV and NHV measure the 3-D roughness of buildings. 3DPLand and 3DLPI were derived from the PLand and LPI, and their abilities were also carried on from 2-D to 3-D spaces. CI measures the vertical development of a parcel or subdistrict. DSM pixels intersecting with building pixels were used to calculate these 3-D landscape metrics of buildings. In particular, the height of the highest building in a unit was

¹[Online]. Available: <http://59.175.109.173:8888/index.html>

²[Online]. Available: www.openstreetmap.org

TABLE I
VARIABLES IN THIS STUDY AT THE PARCEL LEVEL

Type	Variables	Abbreviation	Calculation	Description
2D landscape metrics	Percentage of landscape	PLand	$\frac{\sum_{j=1}^n a_{ij}}{A} \times 100\%$	Measures the proportional abundance of each land cover class in a parcel
	Edge density	ED	$\frac{\sum_{j=1}^n e_{ij}}{A} \times 10000$	Measures the shape complexity degree of each land cover class
	Largest patch index	LPI	$\frac{\max_{j=1}^n (a_{ij})}{A} \times 100\%$	Measures the dominance of each land cover class
	Patch density	PD	$\frac{n_i}{A} \times 10000$	The number of patches on a per unit area
	Percentage of like adjacency	PLADJ	$\frac{g_{ii}}{\sum_{k=1}^l g_{ik}} \times 100\%$	Measures the frequency with which different pairs of land cover types appear side by side
3D landscape metrics	Total volume	TV	$\sum_{k=1}^n v_k$	Total volume of buildings in a parcel
	Mean height	MH	$\frac{\sum_{k=1}^n h_k}{n}$	Mean height of buildings in a parcel
	Height variance	HV	$\frac{1}{n} \sum_{k=1}^n (h_k - MH)^2$	Height variance of buildings in a parcel
	Normalized height variance	NHV	$\frac{\sqrt{HV}}{MH}$	Ratio between the standard deviation of building height and the mean building height in a parcel. It measures the relative height variance
	3D percentage of landscape	3DPLand	$\frac{\sum_{k=1}^n v_k}{V} \times \%$	Measures the 3D proportional abundance of buildings in a parcel
	3D largest patch index	3DLPI	$\frac{\max_{k=1}^n (v_k)}{V} \times 100\%$	Measures the dominance of buildings in a parcel
	Cubic Index	CI	$\frac{TV}{A}$	Ratio of building volume and parcel area
Nighttime light	Average nighttime light	Average NTL	$\frac{\sum_{l=1}^m DN_l}{m}$	The average intensity of nighttime light in a parcel. It represents the socio-economic level of the parcel

Note: a_{ij} = area of patch j in class i , A = parcel area, e_{ij} = total length of the edge in landscape involving patch j in class i , includes landscape boundary and background segments involving patch j , n_i = the number of patches in class i , g_{ii} = the number of adjacent patches of class i , v_k = volume of building k , n = number of buildings in a parcel, V = parcel volume (parcel area multiplied by the height of the highest building in this parcel), h_k = height of building k , DN_l = digital number of NTL pixel l , and m = number of NTL pixels in a parcel.

deemed as the height of this unit when we calculate the unit's volume.

Considering different areas of parcels, we computed the average NTL intensity to represent the socioeconomic levels in every unit. NTL pixels whose most part was covered by a parcel or subdistrict were used for the calculation.

C. Regression Analysis Between 2-D/3-D Landscape Metrics and NTL Intensities With XGBoost

XGBoost, a scalable tree boosting system, is one of the most popular machine learning models in the field of data science. The basic technique of XGBoost is gradient tree boosting, which carries the new weak classification or regression tree into previous models to correct the residuals in the prediction [60]. Tree-based models usually outperform deep models and can be more interpretable than linear models on tabular-style datasets [61], [62], so they are suitable for our dataset. In XGBoost, trees are built sequentially instead of independently, which means that each tree is grown using information from previously grown trees. XGBoost repetitively leverages the patterns in residuals, strengthens the model with weak predictions, and makes it better.

The advantages behind the success of XGBoost include strategies to prevent overfitting, parallelization, sparsity-aware split finding approach, and cache optimization of data structures and algorithms [62]. In this study, we built an XGBoost regression model, in which 2-D/3-D landscape metrics are independent variables and Luojia1-01 NTL intensity is the dependent variable. We first detected the collinearity among all the landscape pattern variables and dropped the collinear variables. The remaining variables were then imported into the XGBoost model to investigate the nonlinear relationship between the landscape pattern variables and NTL intensity. The 1299 and 106 groups of variables in study areas were randomly split into training sets (80%) and test sets (20%).

In the XGBoost regression model, seven parameters we tuned, including the *number of estimators* (from 10 to 1000 with an interval of 1), *maximum depth of a tree* (from 3 to 15 with an interval of 1), *minimum sum of the weights of all observations in a child tree* (from 1 to 6 with an interval of 1), *minimum loss reduction to split a node* (from 0.1 to 0.4 with an interval of 0.1), *sampling rate for each tree* (from 0.6 to 0.9 with an interval of 0.1), *sampling rate for columns of each tree* (from 0.6 to 0.9 at an interval of 0.1), and *weight of L1 regularization* (10-5, 10-2,

0.1, 1, or 100). To build a robust model with XGBoost, we first performed a ten-fold cross-validation to specify the *number of estimators*. After that, we employed a grid search method [63] for tuning of the rest parameters. Grid search scans the whole grid of hyper-param combinations in order, computes the cross-validation loss for each one, and finds the optimal parameter in this manner. After the parameter tuning, the regression model was trained using the training datasets to analyze the relationship between 2-D/3-D landscape metrics and NTL intensity.

D. Regression Model Explanation With SHAP Method

Understanding how and why the model works is as significant as the model's prediction in many applications. However, most machine learning models are so-called "black box" models, where people have no idea how the model makes the input features to the predictions. In this study, we adopted the SHAP method to interpret the correlation between 2-D/3-D landscape metrics and NTL intensity from the well-trained XGBoost model. SHAP method is a game-theoretic approach that can provide explanations for outputs from any machine learning model [64]. The SHAP method gives a SHAP value to measure the importance of each feature for a particular prediction, and features pushing the prediction higher are associated with a positive SHAP value. This local feature explanation method shows better efficiency and consistency than previous similar approaches, such as LIME and DeepLIFT [65], [66]. In this study, SHAP values of 2-D/3-D landscape metrics were calculated to indicate how each metric pushed the NTL intensity positively or negatively. According to the SHAP values, we depicted the summary plot and dependence plots to reveal how these correlations change with the metrics. Metrics in the summary plot were sorted by the sum of SHAP value magnitudes over all samples, thus we could get an overview of which metrics are most important for the model. The dependence plot shows more details by visualizing the contribution of a specific metric.

Moreover, the SHAP method can also calculate the SHAP interaction value to reflect the interaction effects between features and enrich the local explanation. The decomposition of feature impact using SHAP interaction values often reveals interesting hidden relationships. We calculated the SHAP interaction values between each pair of the nine most important 2-D/3-D landscape metrics in every prediction and plotted them in the dependence plots. These interaction values captured the vertical dispersion that was caused by the interaction between metrics and were marked with different colors in the SHAP dependence plot. Summarizing these local explanations, the SHAP method enables us to extend the insights of the model from a local to global view so that we can have a comprehensive understanding of the correlation between landscape patterns and NTL intensity.

IV. RESULTS

A. XGBoost Regression of 2-D/3-D Landscape Metrics and NTL Intensity

To explore the difference between correlations of 2-D and 3-D landscape metrics to NTL intensity, we set up three independent

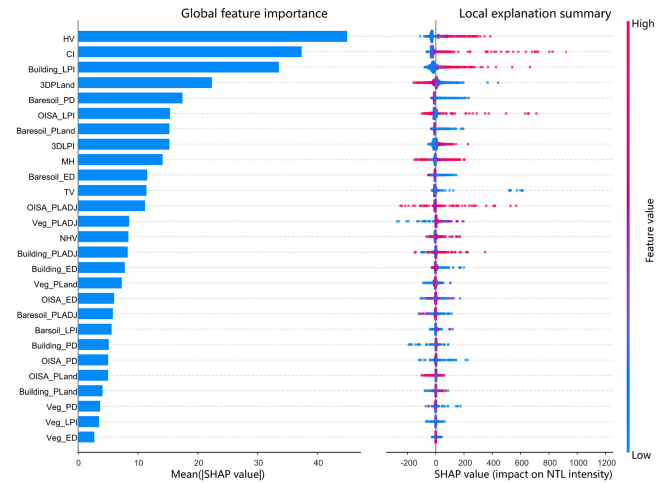


Fig. 3. Parcel level SHAP summary plot of all the landscape metrics in Shanghai city.

variable sets (2-D metrics, 3-D metrics, and all metrics) and built XGBoost regression models, respectively. Seven finetuned parameters in each model were shown in Table II. The coefficient of determination (R^2) on the test sets measuring the proportion of variation that can be explained by the independent variable was used to exam the model's performance.

At the parcel level, the model using all landscape metrics has the best performance with an R^2 of 0.76 and 0.80, respectively, for Shanghai IMC and Beilun district. Combining the 3-D landscape metrics with the 2-D landscape metrics as independent variables improved explained variance of NTL intensity by 5–7%. At the subdistrict level, the model performed best with an R^2 of 0.87 when only 3-D landscape metrics were used, and a slightly lower performance was found when taking both the 2-D and 3-D landscape metrics into account.

B. Contributions of 2-D/3-D Landscape Metrics From SHAP Explanation

For the XGBoost regression model using all variables, the SHAP values of 2-D and 3-D landscape metrics were calculated with the SHAP method. To get an overview of the importance of landscape metrics in the model, we plotted the SHAP values of every metric. The summary plot sorted the metrics by the sum of the SHAP value magnitudes. The blue bars indicate the mean absolute SHAP value of metrics. On the right side of the plot, the SHAP values were used to depict the distribution of the contribution of each metric on the NTL intensity, and the color represents the metric with high values appearing red and low values appearing blue.

At the parcel level, HV, CI, and Building LPI are the top three landscape metrics that have positive contributions to the NTL intensity in Shanghai IMC (see Fig. 3). In other words, the dominance of large buildings has a significantly positive correlation to the NTL intensity in a parcel. On the contrary, vegetation LPI and vegetation ED have the lowest SHAP values that are almost unrelated to the NTL intensity. While in the Beilun district, CI, OISA LPI, and Building PLand were found

TABLE II
TUNED PARAMETERS AND COEFFICIENTS OF DETERMINATION OF XGBOOST REGRESSIONS WITH DIFFERENT VARIABLE SETS

Variable set/Tuned parameters	Number of estimators	Maximum depth of a tree	Minimum sum of the weights of all observations in a child tree	Minimum loss reduction to split a node	Sampling rate for each tree	Sampling rate for columns of each tree	Weight of L1 regularization	R square
Shanghai: Parcel level	2D landscape metrics	23	3	5	0	0.7	0.8	0.1
	3D landscape metrics	16	3	5	0	0.8	0.6	100
	2D and 3D landscape metrics	14	3	5	0	0.9	0.6	1
Ningbo: Parcel level	2D landscape metrics	384	8	5	0	0.9	0.7	100
	3D landscape metrics	42	3	5	0	0.6	0.9	100
	2D and 3D landscape metrics	70	5	5	0.4	0.7	0.9	0.00001
Shanghai: Subdistrict level	2D landscape metrics	15	3	1	0	0.9	0.7	100
	3D landscape metrics	31	6	5	0	0.9	0.9	0.00001
	2D and 3D landscape metrics	24	4	5	0	0.9	0.7	100

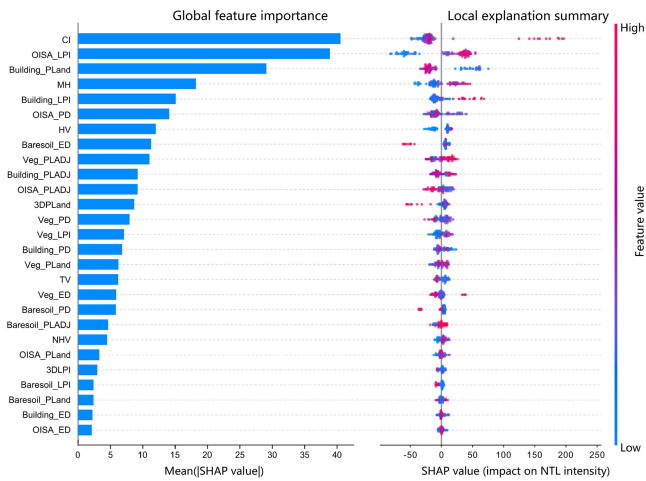


Fig. 4. Parcel level SHAP summary plot of all the landscape metrics in the Beilun district.

to have the most significant contributions to NTL intensity (see Fig. 4). Among them, Building PLand has a significantly negative correlation with NTL intensity, indicating that the larger percentage of building area, the stronger decrement effects of NTL intensity have. Building ED and OSIA ED were found to have the lowest relations to the NTL intensity. For the two study areas, the 10 topmost landscape metrics have larger SHAP values than the last 17.

At the subdistrict level, HV, NHV, and Baresoil PLand are the three topmost landscape metrics that have significant contributions to NTL intensity (see Fig. 5). The metrics having

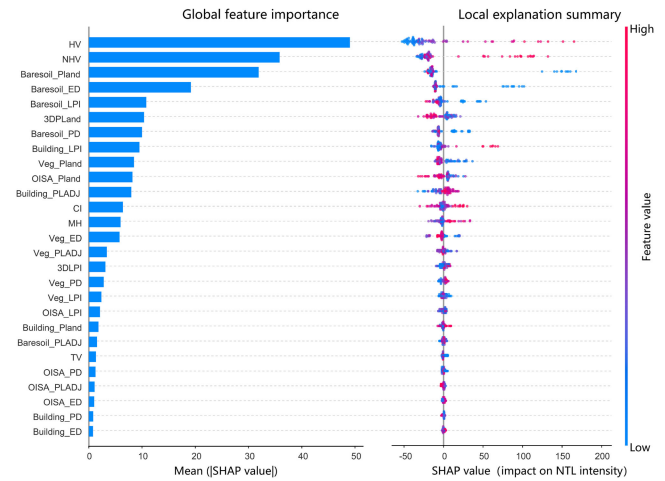


Fig. 5. Subdistrict level SHAP summary plot of all the landscape metrics.

large contributions (e.g., CI and MH) at the parcel level show a moderate contribution to the NTL intensity at the subdistrict level. It is also clear that bare soil-related landscape metrics (e.g., Baresoil ED and LPI) make a significant contribution to NTL intensity at this level. From the distributions of colored SHAP values, the positive or negative effect of the contribution of each metric to the NTL intensity can be identified. The correlations between most landscape metrics and NTL intensity changed as metrics grew, and the greater contribution the metric has, the more obvious the change would be. A detailed discussion of the single metric is presented in Section V-A.

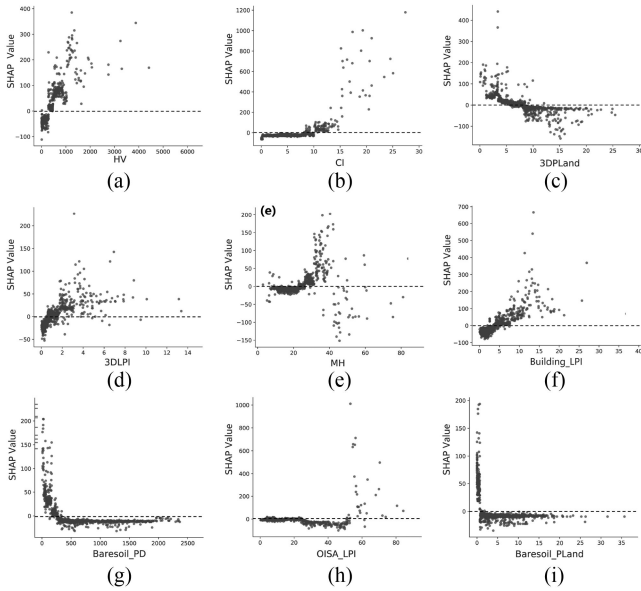


Fig. 6 Parcel level SHAP dependence plots for the nine most influential landscape metrics in Shanghai city.

V. DISCUSSION

A. Relationship Between 2-D/3-D Urban Landscape Metrics and NTL Intensity

The XGBoost regression results show that the urban 2-D and 3-D landscape pattern plays a significant role in urban development. The SHAP summary plot shows the importance of each metric in the regression model and the fact that the contribution of the metric changes with the growing metric value. Based on these understandings, we conducted a further analysis with the SHAP method to explore how these 2-D and 3-D landscape metrics are related to NTL intensity and how they interact with each other, which will advance our knowledge of urban development.

1) *Changing Correlation Between Urban Landscape Pattern and NTL Intensity*: The correlations between urban landscape patterns and their contributions to NTL intensity are not simply positive or negative. Taking the nine 2-D/3-D landscape metrics with the greatest SHAP value magnitudes as an example, we depict the distribution of their SHAP values in SHAP dependence plots to demonstrate how their correlations change (see Fig. 6). In general, as the landscape metric increases, the SHAP value has an obvious critical conversion point that is the threshold of whether the landscape metric has a positive correlation to the NTL intensity. By analyzing the SHAP dependence plot of each landscape metric in detail, we attempted to find out the urban landscape patterns that are closely related to high NTL intensity.

In Shanghai IMC, the four most influential 2-D landscape metrics comprising Building LPI, Bare-soil PD, Bare-soil PLand, and OISA LPI cover three land cover types. Building LPI that measures the dominance of large buildings in a parcel has the greatest contribution to the NTL intensity among all metrics. However, Building PLand that measures the proportion of building in a parcel ranks 24th out of 27 (see Fig. 3). It means that,

at the parcel level in a 2-D space, the contribution of the largest building's dominance on the NTL intensity is much greater than that of building proportion. As Building LPI increases, its SHAP value keeps at a negative value close to 0 first and then begins increasing to a positive value at around 5, which is the threshold of a positive contribution [see Fig. 6(f)]. That is to say at the parcel level, Building LPI cannot advance and even restrain the NTL intensity until it exceeds the threshold, and then its catalytic effect increases with its growth. In short, the high NTL intensity mostly occurred in the parcel with a dominant large building. By contrast, two bare soil metrics have a positive effect when they are very low and then their SHAP values keep steady and negative with their increase [see Fig. 6(g) and (i)]. Thresholds for Baresoil PLand and Baresoil PD are 1 and 75, respectively. The high Bare-soil PLand and Bare-soil PD correspond to the low land use efficiency. In other words, only when the land use efficiency reaches a relatively high level can the NTL intensity be promoted. Then this promotion will have a steep rise with the increase of land use efficiency. As for OISA LPI, it ranks 6th for the importance in the regression model and has a positive correlation with the NTL intensity in the limited parcel when it is greater than 53 [see Fig. 6(h)].

Compared with 2-D landscape metrics, the SHAP value changes of 3-D metrics are more complex. Five building 3-D metrics in the nine most influential landscape metrics are CI, HV, 3DPland, 3DLPI, and MH. There is a significant positive correlation between the HV and its SHAP value [see Fig. 6(a)]. The threshold of the positive effect is around 282. CI, as the ratio of building volume and total landscape area, measures the vertical development level of a parcel in a 3-D space. As the CI grows, its SHAP value increases in three-stage [see Fig. 6(b)]. The first critical point for CI is around 10. When CI increases beyond the first critical point, its SHAP value changes from negative to positive. Then, the positive effect is further amplified when the CI is greater than 15. This result demonstrates that the intensity of NTL is increasing with the vertical development of the parcel. HV measures the 3-D roughness of buildings. Compared with the Building PLand in the 2-D space, 3DPland has a more significant correlation with the NTL intensity (see Fig. 3). The SHAP value of 3DPland decreases with the increase of its value and changes from positive to negative at around 8 [see Fig. 6(c)]. It suggests that the increasing proportion of buildings in the 3-D space will retard its positive effect on NTL development. The SHAP value of 3DLPI increases with its growth and has a similar pattern to the Building LPI [see Fig. 6(d)]. So there is also a positive relationship between the dominance of large buildings and the NTL intensity in the 3-D space. The SHAP value of MH keeps flat and negative first and leaps to the maximum at around 29 m. Then it shows a falling trend but maintains positive [see Fig. 6(e)]. Thus, only when the average height of buildings in a parcel increases to 29 m, can it have a positive effect on the NTL intensity. But the positive effect will be weakened with the building height growing.

For the Beilun district, nine landscape metrics, including CI, MH, HV, OISA_LPI, Building_PLand, Building LPI, OISA_PD, Baresoil_ED, and Veg_PLADJ, which are found to have significant contributions to the NTL intensity were selected

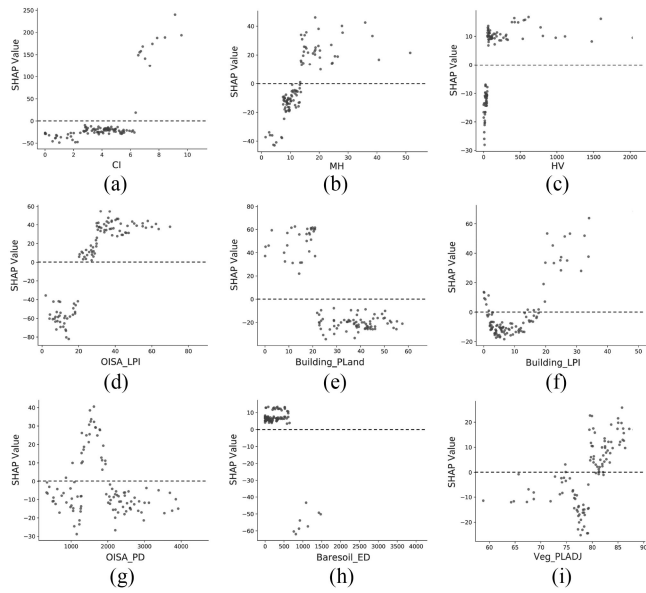


Fig. 7 Parcel level SHAP dependence plots for the nine most influential landscape metrics in Beilun district.

to show their SHAP dependence plots. As shown in Fig. 7, more dispersed scatter plots can be observed compared with that of Shanghai city. A positive effect of CI is significant in specification 6.3 [see Fig. 7(a)], thus an increase in CI value will increase the NTL intensity. This effect can be explained that the vertical development at parcel levels will advance the promotion of NTL intensity. As shown in Fig. 7(b), the effect of MH turns positive in the specification of 14, and then an increase of MH will increase the NTL intensity. While a stable effect can be observed when the HV value exceeds 65 [Fig. 7(c)]. This indicates that the fluctuations of building heights are more significant in the developed regions. OISA LPI has a positive effect when its value exceeds 20 [see Fig. 7(d)], and then an increase in OISA LPI value will increase the NTL intensity. Large OISA LPI, which means large-scale urban construction, will speed up the pace to increase the NTL intensity. As shown in Fig. 7(f), an interesting “V” distribution can be observed in the SHAP dependence plot of Building LPI. This means that at the parcel level, the increase of small buildings has a significant effect on the increase of NTL intensity at the earlier stage, while the contributions of large buildings on the urban socioeconomic development become more important when the buildings increase to a certain level.

Combining the analyses of 2-D and 3-D landscape metrics, we can infer the characteristics of urban landscape patterns that have a positive correlation with the NTL intensity in a parcel: large building (high Building LPI and 3DLPI), high land use efficiency (low Baresoil PLand and Baresoil PD), extensive vertical development (high CI and MH), and great building roughness and diversity (high HV and low 3DPLand). According to these characteristics, two typical parcels were selected as samples to further explore more detailed information. The first parcel meets all positive characteristics and has higher NTL intensity [see Fig. 8(a)]. Shopping malls, office buildings, and

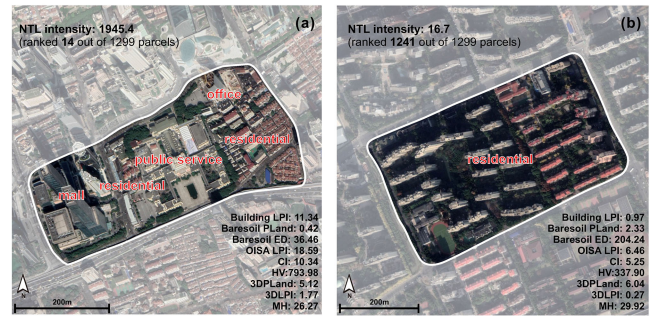


Fig. 8 Aerial photos of two typical parcels: (a) with landscape patterns that boost the urban socioeconomic level, and (b) with landscape patterns that inhibit the urban socioeconomic level.

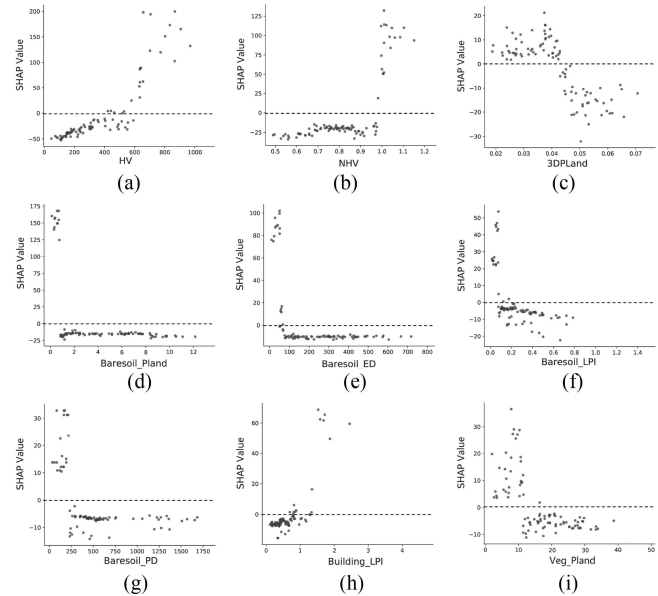


Fig. 9. Subdistrict level SHAP dependence plots for the nine most influential landscape metrics.

public service facilities are distributed around residential areas in this parcel. And the diversity of buildings and the mixed land uses provide multiple urban functions. This landscape pattern is in line with the concept of a compact city that is considered a valid sustainable model for urban development [66], [67]. In the second parcel, all buildings are residential and their distribution is relatively loose [see Fig. 8(b)]. Although it is a rich neighborhood and close to the Lujiazui financial center, its NTL intensity is low.

Fig. 9 shows the top nine landscape metrics which have the greatest SHAP value magnitudes at the subdistrict level. It was found that Building HV and NHV have large threshold values which turn from a negative contribution to a positive contribution on NTL intensity. In other words, at the subdistrict level, only large building height variations make positive contributions to NTL intensity. Building LPI and bare soil-related landscape metrics show similar contributions on the NTL intensity at both subdistrict and parcel levels. Vegetation PLand [see Fig. 9(i)] also makes a certain contribution to the NTL intensity. As the Vegetation PLand increases, its SHAP value decreases and turns

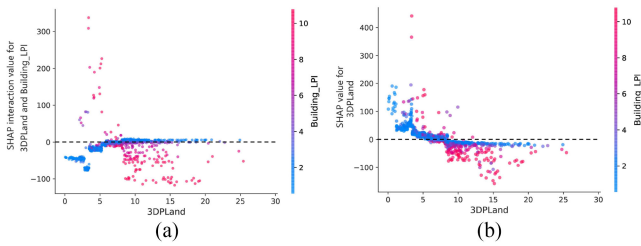


Fig. 10 SHAP interaction plots and dependence plots with interaction for two pairs of landscape metrics with strong interaction.

negative when Vegetation PLand reaches 11. In total, although the contribution degree of some landscape metrics to NTL intensity has descended at the subdistrict level, the change in the trend direction is the same as that at the parcel level. The landscape metrics that make positive contributions to the NTL intensity are almost the same at the two different levels.

It should also be noted that previous studies [51], [52] suggested that the viewing zenith angle (the angle between the line of sight to the satellite and local zenith) of Suomi-NPP satellite is one of the major factors influencing the NTL intensity variation in highly urbanized areas. The nonlinear relationship between NTL intensity and viewing angle varies with different urban morphology characteristics. NTL intensity has been shown to increase toward higher viewing zenith angles over residential areas, while the opposite trend is often found across dense urban centers [52]. Therefore, the angle-radiance relationship may have certain impacts on our study addressing linkages between urban 2-D/3-D landscape pattern and NTL intensity, which requires further research.

2) Interactions Between 2-D/3-D Urban Landscape Metrics:

The NTL intensity is not only related to the single landscape metric but sometimes tends to be the result of metrics interaction. To discover the hidden relationship between 2-D/3-D landscape metrics, SHAP interaction values were computed between the nine most influential landscape metrics. A typical group of interaction landscape metrics is 3DPLand and Building LPI. Depending on whether there is a large building in a parcel, the interaction value between 3DPLand and Building LPI shows different patterns [see Fig. 10(a)]. For parcels with large buildings [points close to red in Fig. 6(a)], the interaction is very strong in the low-value region of 3DPLand and then shows a rapid decline as the 3DPLand increases. But for parcels without large buildings [points close to blue in Fig. 10(a)], the interaction value grows gently from negative to zero. The effects of these different interactions on SHAP values of 3DPLand can be observed by recoloring the SHAP dependence plot of 3DPLand [see Fig. 10(b)]. Since the blue points in Fig. 10(b) is much flatter than the red points, the proportion of buildings in the 3-D space has a more critical correlation with the NTL intensity for a parcel that is dominated by a large building than that has no significant large building.

B. Implications for Urban Planning and Management

Smart utilization of the knowledge of urban 2-D and 3-D landscape patterns can coordinate the urban spatial and

socioeconomic development and alleviate the unsustainable problems caused by rapid urbanization. Based on findings in this study, we would suggest a few strategies for urban planners at the parcel level. First, a large building in a parcel is the significant driving force of socioeconomic development. Large buildings are often the urban or regional function center, where a large number of socioeconomic activities take place. With the urban development, large buildings transform from the single-functional center to the multifunctional city complex, which is a larger scale economic aggregate in developed cities. Second, persisting in compact city development contributes to urban socioeconomic and sustainable development. According to Section V, the landscape patterns of the compact city, such as mixed land use and intensive use of land resources, have a positive correlation with NTL intensity.

VI. CONCLUSION

This article applied the XGBoost regression to establish the correlation between 2-D/3-D urban landscape patterns and NTL intensity at the parcel and subdistrict scales. The regression model shows that both the 2-D and 3-D landscape patterns have a significant correlation with NTL intensity. According to the SHAP method, we found that the proportion of buildings in either the 2-D or 3-D space has little relation to NTL intensity. The dominance of large buildings plays an important role in improving the NTL intensity. In addition, improving the roughness and diversity of buildings can be beneficial to the increase of NTL intensity. For urban vertical development, the average height of the buildings makes a positive contribution to the NTL intensity until it reaches a threshold, however, this positive effect is weakened with the increase of the building height. We hope our findings could provide a better understanding of urban development for urban planners and governments so that the goal of urban sustainable development is closer.

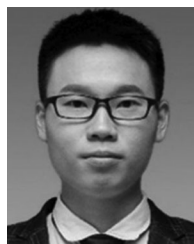
This work can be extended in several ways. First, more additional landscape metrics can be incorporated into the machine learning models to produce a more comprehensive profile of the urban physical environment. Another interesting extension of this study would be a further investigation to explore the relationships between landscape patterns and NTL intensity in other cities, and thus gives a more comprehensive explanation of the mechanism between the 2-D/3-D landscape pattern variables and the average NTL intensity.

REFERENCES

- [1] United Nations, San Francisco, CA, USA, 2018 Revision of World Urbanization Prospects, 2018.
- [2] A. Y. Hoekstra and T. O. Wiedmann, "Humanity's unsustainable environmental footprint," *Science*, vol. 344, no. 6188, pp. 1114–1117, 2014, doi: [10.1126/science.1248365](https://doi.org/10.1126/science.1248365).
- [3] U. Al-Mulali, I. Ozturk, and H. H. Lean, "The influence of economic growth, urbanization, trade openness, financial development, and renewable energy on pollution in Europe," *Natural Hazards*, vol. 79, no. 1, pp. 621–644, 2015, doi: [10.1007/s11069-015-1865-9](https://doi.org/10.1007/s11069-015-1865-9).
- [4] I. Pikaar, K. R. Sharma, S. H. Hu, W. Gernjak, J. Keller, and Z. G. Yuan, "Reducing sewer corrosion through integrated urban water management," *Science*, vol. 345, no. 6198, pp. 812–814, 2014, doi: [10.1126/science.1251418](https://doi.org/10.1126/science.1251418).

- [5] B. J. He, J. Wang, H. Liu, and G. Ulpiani, "Localized synergies between heat waves and urban heat islands: Implications on human thermal comfort and urban heat management," *Environ. Res.*, vol. 193, 2021, Art. no. 110584, doi: [10.1016/j.envres.2020.110584](https://doi.org/10.1016/j.envres.2020.110584).
- [6] J. Yang, Y. Yang, D. Sun, C. Jin, and X. Xiao, "Influence of urban morphological characteristics on thermal environment," *Sustain. Cities Soc.*, vol. 72, 2021, Art. no. 103045, doi: [10.1016/j.scs.2021.103045](https://doi.org/10.1016/j.scs.2021.103045).
- [7] J. Yang *et al.*, "Optimizing local climate zones to mitigate urban heat island effect in human settlements," *J. Clean. Prod.*, vol. 275, 2020, Art. no. 123767, doi: [10.1016/j.jclepro.2020.123767](https://doi.org/10.1016/j.jclepro.2020.123767).
- [8] J. Yang *et al.*, "Understanding land surface temperature impact factors based on local climate zones," *Sustain. Cities Soc.*, vol. 69, 2021, Art. no. 102818, doi: [10.1016/j.scs.2021.102818](https://doi.org/10.1016/j.scs.2021.102818).
- [9] H. W. Richardson, "Theory of the distribution of city sizes: Review and prospects," *Regional Stud.*, vol. 7, no. 3, pp. 239–251, 1973, doi: [10.1080/09595237300185241](https://doi.org/10.1080/09595237300185241).
- [10] B. Begović, "Industrial diversification and city size: The case of Yugoslavia," *Urban Stud.*, vol. 29, no. 1, pp. 77–88, 1992, doi: [10.1080/00420989220080061](https://doi.org/10.1080/00420989220080061).
- [11] J. Friedmann, "The spatial organization of power in the development of urban systems," *Develop. Change*, vol. 4, no. 3, pp. 12–50, 1973, doi: [10.1111/j.1467-7660.1973.tb00643.x](https://doi.org/10.1111/j.1467-7660.1973.tb00643.x).
- [12] C. Yang *et al.*, "A spatial-socioeconomic urban development status curve from NPP-VIIRS nighttime light data," *Remote Sens.*, vol. 11, no. 20, 2019, Art. no. 2398, doi: [10.3390/rs11202398](https://doi.org/10.3390/rs11202398).
- [13] X. Bai, J. Chen, and P. Shi, "Landscape urbanization and economic growth in China: Positive feedbacks and sustainability dilemmas," *Environ. Sci. Technol.*, vol. 46, no. 1, pp. 132–139, 2012, doi: [10.1021/es202329f](https://doi.org/10.1021/es202329f).
- [14] K. Shi, J. Shen, L. Wang, M. Ma, and Y. Cui, "A multiscale analysis of the effect of urban expansion on PM_{2.5} concentrations in China: Evidence from multisource remote sensing and statistical data," *Building Environ.*, vol. 174, 2020, Art. no. 106788, doi: [10.1016/j.buildenv.2020.106788](https://doi.org/10.1016/j.buildenv.2020.106788).
- [15] C. C. Fan, "The vertical and horizontal expansions of China's city system," *Urban Geography*, vol. 20, no. 6, pp. 493–515, 1999, doi: [10.2747/0272-3638.20.6.493](https://doi.org/10.2747/0272-3638.20.6.493).
- [16] S. Frolking, T. Milliman, K. C. Seto, and M. A. Friedl, "A global fingerprint of macro-scale changes in urban structure from 1999 to 2009," *Environ. Res. Lett.*, vol. 8, no. 2, 2013, Art. no. 024004, doi: [10.1088/1748-9326/8/2/024004](https://doi.org/10.1088/1748-9326/8/2/024004).
- [17] B. Yu, H. Liu, J. Wu, Y. Hu, and L. Zhang, "Automated derivation of urban building density information using airborne LiDAR data and object-based method," *Landscape Urban Planning*, vol. 98, no. 3/4, pp. 210–219, 2010, doi: [10.1016/j.landurbplan.2010.08.004](https://doi.org/10.1016/j.landurbplan.2010.08.004).
- [18] B. Wu *et al.*, "An extended minimum spanning tree method for characterizing local urban patterns," *Int. J. Geographical Inf. Sci.*, vol. 32, no. 3, pp. 450–475, 2018, doi: [10.1080/13658816.2017.1384830](https://doi.org/10.1080/13658816.2017.1384830).
- [19] B. Wu *et al.*, "A graph-based approach for 3D building model reconstruction from airborne LiDAR point clouds," *Remote Sens.*, vol. 9, no. 1, 2017, doi: [10.3390/rs9010092](https://doi.org/10.3390/rs9010092).
- [20] B. Wu *et al.*, "Mapping fine-scale visual quality distribution inside urban streets using mobile LiDAR data," *Building Environ.*, vol. 206, 2021, doi: [10.1016/j.buildenv.2021.108323](https://doi.org/10.1016/j.buildenv.2021.108323).
- [21] W. Zhang, W. Li, C. Zhang, and W. B. Ouimet, "Detecting horizontal and vertical urban growth from medium resolution imagery and its relationships with major socioeconomic factors," *Int. J. Remote Sens.*, vol. 38, no. 12, pp. 3704–3734, 2017, doi: [10.1080/01431161.2017.1302113](https://doi.org/10.1080/01431161.2017.1302113).
- [22] I. Zambon, A. Colantoni, and L. Salvati, "Horizontal vs vertical growth: Understanding latent patterns of urban expansion in large metropolitan regions," *Sci. Total Environ.*, vol. 654, pp. 778–785, 2019, doi: [10.1016/j.scitotenv.2018.11.182](https://doi.org/10.1016/j.scitotenv.2018.11.182).
- [23] S. Yu *et al.*, "Exploring the relationship between 2D/3D landscape pattern and land surface temperature based on explainable eXtreme gradient boosting tree: A case study of Shanghai, China," *Sci. Total Environ.*, vol. 725, 2020, Art. no. 138229, doi: [10.1016/j.scitotenv.2020.138229](https://doi.org/10.1016/j.scitotenv.2020.138229).
- [24] P. Martin, Y. Baudouin, and P. Gachon, "An alternative method to characterize the surface urban heat island," *Int. J. Biometeorol.*, vol. 59, no. 7, pp. 849–861, 2015, doi: [10.1007/s00484-014-0902-9](https://doi.org/10.1007/s00484-014-0902-9).
- [25] T. van Hooff and B. Blocken, "Coupled urban wind flow and indoor natural ventilation modelling on a high-resolution grid: A case study for the Amsterdam ArenA stadium," *Environ. Model. Softw.*, vol. 25, no. 1, pp. 51–65, 2010, doi: [10.1016/j.envsoft.2009.07.008](https://doi.org/10.1016/j.envsoft.2009.07.008).
- [26] K. C. Seto and M. Fragkias, "Quantifying spatiotemporal patterns of urban land-use change in four cities of China with time series landscape metrics," *Landscape Ecol.*, vol. 20, no. 7, pp. 871–888, 2005, doi: [10.1007/s10980-005-5238-8](https://doi.org/10.1007/s10980-005-5238-8).
- [27] C. Fang, G. Li, and S. Wang, "Changing and differentiated urban landscape in China: Spatiotemporal patterns and driving forces," *Environ. Sci. Technol.*, vol. 50, no. 5, pp. 2217–2227, 2016, doi: [10.1021/acs.est.5b05198](https://doi.org/10.1021/acs.est.5b05198).
- [28] Q. Wu, F. X. Guo, H. Q. Li, and J. Y. Kang, "Measuring landscape pattern in three dimensional space," *Landscape Urban Planning*, vol. 167, pp. 49–59, 2017, doi: [10.1016/j.landurbplan.2017.05.022](https://doi.org/10.1016/j.landurbplan.2017.05.022).
- [29] X. Huang and Y. Wang, "Investigating the effects of 3D urban morphology on the surface urban heat island effect in urban functional zones by using high-resolution remote sensing data: A case study of Wuhan, Central China," *ISPRS J. Photogrammetry Remote Sens.*, vol. 152, pp. 119–131, 2019, doi: [10.1016/j.isprsjprs.2019.04.010](https://doi.org/10.1016/j.isprsjprs.2019.04.010).
- [30] C. Berger, J. Rosentreter, M. Voltersen, C. Baumgart, C. Schullius, and S. Hese, "Spatio-temporal analysis of the relationship between 2D/3D urban site characteristics and land surface temperature," *Remote Sens. Environ.*, vol. 193, pp. 225–243, 2017, doi: [10.1016/j.rse.2017.02.020](https://doi.org/10.1016/j.rse.2017.02.020).
- [31] C. D. Elvidge, K. E. Baugh, E. A. Kihn, H. W. Kroehl, and E. R. Davis, "Mapping city lights with nighttime data from the DMSP operational linescan system," *Photogrammetry Eng. Remote Sens.*, vol. 63, no. 6, pp. 727–734, 1997.
- [32] C. D. Elvidge *et al.*, "The Nightsat Mission concept," *Int. J. Remote Sens.*, vol. 28, no. 12, pp. 2645–2670, 2007, doi: [10.1080/01431160600981525](https://doi.org/10.1080/01431160600981525).
- [33] P. Sutton, D. Roberts, C. Elvidge, and K. Baugh, "Census from heaven: An estimate of the global human population using nighttime satellite imagery," *Int. J. Remote Sens.*, vol. 22, no. 16, pp. 3061–3076, 2001.
- [34] C. D. Elvidge, K. E. Baugh, E. A. Kihn, H. W. Kroehl, E. R. Davis, and C. W. Davis, "Relation between satellite observed visible-near infrared emissions, population, economic activity and electric power consumption," *Int. J. Remote Sens.*, vol. 18, no. 6, pp. 1373–1379, 1997, doi: [10.1080/014311697218485](https://doi.org/10.1080/014311697218485).
- [35] K. Shi *et al.*, "Evaluating the ability of NPP-VIIRS nighttime light data to estimate the gross domestic product and the electric power consumption of China at multiple scales: A comparison with DMSP-OLS data," *Remote Sens.*, vol. 6, no. 2, pp. 1705–1724, 2014, doi: [10.3390/rs6021705](https://doi.org/10.3390/rs6021705).
- [36] N. Zhao, Y. Liu, G. Cao, E. L. Samson, and J. Zhang, "Forecasting China's GDP at the pixel level using nighttime lights time series and population images," *GISci. Remote Sens.*, vol. 54, no. 3, pp. 407–425, 2017, doi: [10.1080/15481603.2016.1276705](https://doi.org/10.1080/15481603.2016.1276705).
- [37] K. Shi *et al.*, "Modeling spatiotemporal CO₂ (carbon dioxide) emission dynamics in China from DMSP-OLS nighttime stable light data using panel data analysis," *Appl. Energy*, vol. 168, pp. 523–533, 2016, doi: [10.1016/j.apenergy.2015.11.055](https://doi.org/10.1016/j.apenergy.2015.11.055).
- [38] X. Zhang, J. Wu, J. Peng, and Q. Cao, "The uncertainty of nighttime light data in estimating carbon dioxide emissions in China: A comparison between DMSP-OLS and NPP-VIIRS," *Remote Sens.*, vol. 9, no. 8, 2017, doi: [10.3390/rs9080797](https://doi.org/10.3390/rs9080797).
- [39] K. Shi *et al.*, "Detecting spatiotemporal dynamics of global electric power consumption using DMSP-OLS nighttime stable light data," *Appl. Energy*, vol. 184, pp. 450–463, 2016, doi: [10.1016/j.apenergy.2016.10.032](https://doi.org/10.1016/j.apenergy.2016.10.032).
- [40] M. Mann, E. Melaas, and A. Malik, "Using VIIRS day/night band to measure electricity supply reliability: Preliminary results from Maharashtra, India," *Remote Sens.*, vol. 8, no. 9, 2016, doi: [10.3390/rs8090711](https://doi.org/10.3390/rs8090711).
- [41] J. R. Tian, N. Z. Zhao, E. L. Samson, and S. L. Wang, "Brightness of nighttime lights as a proxy for freight traffic: A case study of China," *IEEE J. Sel. Topics Appl. Earth Observ. Remote Sens.*, vol. 7, no. 1, pp. 206–212, Jan. 2014.
- [42] K. Shi *et al.*, "Modeling and mapping total freight traffic in China using NPP-VIIRS nighttime light composite data," *GISci. Remote Sens.*, vol. 52, no. 3, pp. 274–289, 2015, doi: [10.1080/15481603.2015.1022420](https://doi.org/10.1080/15481603.2015.1022420).
- [43] Z. Q. Chen *et al.*, "A new approach for detecting urban centers and their spatial structure with nighttime light remote sensing," *IEEE Trans. Geosci. Remote Sens.*, vol. 55, no. 11, pp. 6305–6319, Nov. 2017.
- [44] B. Wu *et al.*, "A surface network based method for studying urban hierarchies by night time light remote sensing data," *Int. J. Geographical Inf. Sci.*, vol. 33, no. 7, pp. 1377–1398, 2019, doi: [10.1080/13658816.2019.1585540](https://doi.org/10.1080/13658816.2019.1585540).
- [45] B. Yu, K. Shi, Y. Hu, C. Huang, Z. Chen, and J. Wu, "Poverty evaluation using NPP-VIIRS nighttime light composite data at the county level in China," *IEEE J. Sel. Topics Appl. Earth Observ. Remote Sens.*, vol. 8, no. 3, pp. 1217–1229, Mar. 2015.
- [46] N. Jean, M. Burke, M. Xie, W. M. Davis, D. B. Lobell, and S. Ermon, "Combining satellite imagery and machine learning to predict poverty," *Science*, vol. 353, no. 6301, pp. 790–794, Aug. 2016, doi: [10.1126/science.aaf7894](https://doi.org/10.1126/science.aaf7894).

- [47] K. Shi, Z. Chang, Z. Chen, J. Wu, and B. Yu, "Identifying and evaluating poverty using multisource remote sensing and point of interest (POI) data: A case study of Chongqing, China," *J. Cleaner Prod.*, vol. 255, 2020, Art. no. 120245, doi: [10.1016/j.jclepro.2020.120245](https://doi.org/10.1016/j.jclepro.2020.120245).
- [48] C. Wang *et al.*, "Analyzing parcel-level relationships between Luojia 1-01 nighttime light intensity and artificial surface features across Shanghai, China: A comparison with NPP-VIIRS data," *Int. J. Appl. Earth Obs. Geoinf.*, vol. 85, 2020, Art. no. 101989, doi: [10.1016/j.jag.2019.101989](https://doi.org/10.1016/j.jag.2019.101989).
- [49] X. Li, X. Li, D. Li, X. He, and M. Jendryke, "A preliminary investigation of Luojia-1 night-time light imagery," *Remote Sens. Lett.*, vol. 10, no. 6, pp. 526–535, 2019, doi: [10.1080/2150704x.2019.1577573](https://doi.org/10.1080/2150704x.2019.1577573).
- [50] G. Zhang, L. Li, Y. Jiang, X. Shen, and D. Li, "On-orbit relative radiometric calibration of the night-time sensor of the Luojia1-01 satellite," *Sensors*, vol. 18, no. 12, 2018, Art. no. 4225, doi: [10.3390/s18124225](https://doi.org/10.3390/s18124225).
- [51] X. Li *et al.*, "Anisotropic characteristic of artificial light at night – systematic investigation with VIIRS DNB multi-temporal observations," *Remote Sens. Environ.*, vol. 233, 2019, Art. no. 111357, doi: [10.1016/j.rse.2019.111357](https://doi.org/10.1016/j.rse.2019.111357).
- [52] Z. Wang *et al.*, "Quantifying uncertainties in nighttime light retrievals from Suomi-NPP and NOAA-20 VIIRS day/night band data," *Remote Sens. Environ.*, vol. 263, 2021, Art. no. 112557, doi: [10.1016/j.rse.2021.112557](https://doi.org/10.1016/j.rse.2021.112557).
- [53] Q. Zheng *et al.*, "A new source of multi-spectral high spatial resolution night-time light imagery—JL1-3B," *Remote Sens. Environ.*, vol. 215, pp. 300–312, 2018, doi: [10.1016/j.rse.2018.06.016](https://doi.org/10.1016/j.rse.2018.06.016).
- [54] T. Hu, J. Yang, X. Li, and P. Gong, "Mapping urban land use by using landsat images and open social data," *Remote Sens.*, vol. 8, no. 2, 2016, Art. no. 151, doi: [10.3390/rs8020151](https://doi.org/10.3390/rs8020151).
- [55] B. Wu, B. Yu, Q. Wu, Y. Huang, Z. Chen, and J. Wu, "Individual tree crown delineation using localized contour tree method and airborne LiDAR data in coniferous forests," *Int. J. Appl. Earth Obs.*, vol. 52, pp. 82–94, 2016, doi: [10.1016/j.jag.2016.06.003](https://doi.org/10.1016/j.jag.2016.06.003).
- [56] X. Huang, H. Chen, and J. Gong, "Angular difference feature extraction for urban scene classification using ZY-3 multi-angle high-resolution satellite imagery," *ISPRS J. Photogrammetry Remote Sens.*, vol. 135, pp. 127–141, 2018, doi: [10.1016/j.isprsjprs.2017.11.017](https://doi.org/10.1016/j.isprsjprs.2017.11.017).
- [57] C. Liu, X. Huang, Z. Zhu, H. Chen, X. Tang, and J. Gong, "Automatic extraction of built-up area from ZY3 multi-view satellite imagery: Analysis of 45 global cities," *Remote Sens. Environ.*, vol. 226, pp. 51–73, 2019, doi: [10.1016/j.rse.2019.03.033](https://doi.org/10.1016/j.rse.2019.03.033).
- [58] X. Huang *et al.*, "High-resolution urban land-cover mapping and landscape analysis of the 42 major cities in China using ZY-3 satellite images," *Sci. Bull.*, vol. 65, no. 12, pp. 1039–1048, 2020, doi: [10.1016/j.scib.2020.03.003](https://doi.org/10.1016/j.scib.2020.03.003).
- [59] K. McGarigal, S. A. Cushman, and E. Ene, "FRAGSTATS v4: spatial pattern analysis program for categorical and continuous maps," Univ. Massachusetts, Amherst, MA, USA. [Online]. Available: www.umass.edu/landeco/research/fragstats/fragstats.html
- [60] J. Friedman, T. Hastie, and R. Tibshirani, "Additive logistic regression: A statistical view of boosting," *Ann. Statist.*, vol. 28, pp. 337–407, 2000, doi: [10.1214/aos/1016218223](https://doi.org/10.1214/aos/1016218223).
- [61] S. Haufe *et al.*, "On the interpretation of weight vectors of linear models in multivariate neuroimaging," *Neuroimage*, vol. 87, pp. 96–110, 2014, doi: [10.1016/j.neuroimage.2013.10.067](https://doi.org/10.1016/j.neuroimage.2013.10.067).
- [62] T. Chen and C. Guestrin, "XGBoost: A scalable tree boosting system," in *Proc. 22nd ACM SIGKDD Int. Conf. Knowl. Discov. Data Mining*, 2016, pp. 785–794.
- [63] P. Fabian *et al.*, "Scikit-learn: Machine learning in Python," *J. Mach. Learn. Res.*, vol. 12, no. 85, pp. 2825–2830, 2011.
- [64] S. M. Lundberg and S.-I. Lee, "A unified approach to interpreting model predictions," in *Proc. 31st Int. Conf. Neural Inf. Process. Syst.*, 2017, pp. 4768–4777.
- [65] S. M. Lundberg *et al.*, "From local explanations to global understanding with explainable AI for trees," *Nature Mach. Intell.*, vol. 2, no. 1, pp. 2522–5839, 2020.
- [66] S. E. Bibri, "Compact urbanism and the synergic potential of its integration with data-driven smart urbanism: An extensive interdisciplinary literature review," *Land Use Policy*, vol. 97, 2020, Art. no. 104703, doi: [10.1016/j.landusepol.2020.104703](https://doi.org/10.1016/j.landusepol.2020.104703).
- [67] W. Musakwa and A. V. Niekerk, "Implications of land use change for the sustainability of urban areas: A case study of Stellenbosch, South Africa," *Cities*, vol. 32, pp. 143–156, 2013, doi: [10.1016/j.cities.2013.01.004](https://doi.org/10.1016/j.cities.2013.01.004).



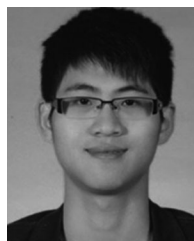
Bin Wu received the Ph.D. degree in cartography and geographic information systems from East China Normal University, Shanghai, China, in 2018.

He is currently an Associate Research Fellow with the East China Normal University. His research interests include urban remote sensing, LiDAR, and spatiotemporal analysis.



Chengshu Yang received the B.S. degree in marine technology from Shanghai Ocean University, Shanghai, China, in 2013, and the Ph.D. degree in cartography and geographic information system from East China Normal University, Shanghai, China, in 2021.

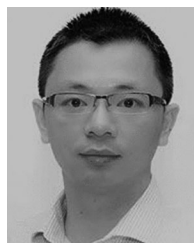
He is currently a Senior Pre-Sales Manager with the Piesat Information Technology Co., Ltd. His research interests include nighttime light remote sensing and its application in urban research.



Zuoqi Chen (Member, IEEE) received the B.S. degree in geographic information system from Fujian Normal University, Fuzhou, China, in 2011, and the Ph.D. degree in cartography and geographic information system from East China Normal University, Shanghai, China, in 2017.

He is currently an Assistant Research Fellow with the Key Laboratory of Spatial Data Mining and Information Sharing of the Ministry of Education, and the Academy of Digital China, Fuzhou University, Fuzhou. His research interests include urban remote

sensing, nighttime light remote sensing, and the development of geographic information system.



Qiusheng Wu received the Ph.D. degree in geography from the University of Cincinnati, Cincinnati, OH, USA, in 2015.

He is currently an Assistant Professor with the Department of Geography, University of Tennessee, Knoxville, TN, USA. His research interests include remote sensing, open-source GIS, wetland hydrology, and Google Earth Engine.



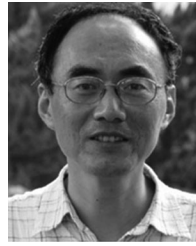
Siyi Yu received the B.S. and the Ph.D. degrees in cartography and geographic information system from East China Normal University, Shanghai, China, in 2013 and 2020, respectively.

Her research interests include spatial data mining and application of GIS, and remote-sensing in urban research.



Congxiao Wang received the B.S. and M.S. degrees in cartography and geographic information system from Shanghai Normal University, Shanghai, China, in 2014 and 2017, respectively. She is currently working toward the Ph.D. degree in cartography and geographic information system with East China Normal University, Shanghai, China.

Her research interests include nighttime light remote sensing and its application in urban research.



Jianping Wu received the M.S. degree in cartography and remote sensing from Peking University, Beijing, China, in 1986, and the Ph.D. degree in regional geography from East China Normal University, Shanghai, China, in 1996.

He is currently a Professor with East China Normal University. His research interests include remote sensing and geographic information system.



Qiaoxuan Li received the B.S. and M.S. degrees in cartography and geographic information system from Fujian Normal University, Fuzhou, China, in 2015 and 2018, respectively. He is currently working toward the Ph.D. degree in cartography and geographic information system with East China Normal University, Shanghai, China.

His research interests include nighttime light remote sensing and its application in urban research.



Bailang Yu (Senior Member, IEEE) received the B.S. and Ph.D. degrees in cartography and geographic information systems from East China Normal University, Shanghai, China, in 2002 and 2009, respectively.

He is currently a Professor with the Key Laboratories of Geographic Information Science, Ministry of Education, and the School of Geographic Sciences, East China Normal University. His research interests include urban remote sensing, nighttime light remote sensing, LiDAR, and object-based methods.